論文の内容の要旨

Thesis Summary

論文題目　Ultrasound waveform tomography with the ring transducer for the breast imaging

（乳房イメージングのためのリングトランスデューサーによる超音波波形トモグラフィー）

氏　名　林　宏翔

1 Introduction

Ultrasound computed tomography (USCT) is a prospective modality for breast cancer diagnosis providing three kinds of three-dimensional images related to the acoustic coefficients: speed of sound, attenuation, and reflection. The classical ultrasound imaging utilizes the reconstruction of acoustic impedance to perform the structure of breast tissues by the use of echo. On the contrary, the reconstruction for quantitative imaging, i.e. speed of sound and attenuation, identifies the spatial distribution for the different types of breast tissues other than the structure. It is roughly classified into two categories: ray-based tomography and waveform tomography. In terms of ray-based tomography, for instance, Qu et al. [7, 8] reconstructs the speed-of-sound images on a ring-transducer imaging system using Fermat's principle for ray tracing. On the other hand, waveform tomography, based on the wave equation retaining the integrated feature of acoustic wave, allows us to reconstruct the high-resolution and accurate images; see [9, 4, 15, 10]. Duric et al. [3] develops a commercial ultrasound tomography imaging system named *SoftVue* and demonstrates that the clinical studies of reconstructing the USCT images by means of waveform tomography. Compared with ray-based tomography, the images of the breast tissue reconstructed by waveform tomography have an advantage of higher resolution and accuracy. However, it is always time-consuming because of a large number of iterations as well as grid points. The contrast source inversion (CSI) method is a kind of inversion methods for ultrasound waveform tomography that does not require the forward solver through the reconstruction [13]. It is able to be calculated on a coarse grid because of the explicit introduction of the Green's function; see [2, 16]. In the literature, there have existed various extensions for the CSI method, such as extended contrast source inversion [14], finite-difference contrast source inversion [1], etc. Ozmen [6] published the pioneer work on the inversion of speed of sound using the CSI method applied to low-frequency data, in terms of breast cancer detection.

The objective of this thesis is to find an effective, efficient, and applicable way to implement the CSI method in the real configuration of the ring-transducer diagnostic device. One can consider more practically that the proposed CSI method stipulates to reconstruct the robust result whenever the raw data with the unknown noise level are applied. One attempts to make full use of the abundant frequency components from dataset for the sake of alleviating the computational cost as well as enhancing the resolution of speed-of-sound reconstruction. Henceforth, one shows a way to process the raw data while employing the CSI method and propose the multi-frequency accelerating strategy. Additionally, the study of calibration as well as the processing of the experimental data are proposed. The phantom image based on the processed data is reconstructed and assessed from the clinical view.

2 Ultrasound waveform tomography with point sources/receivers

The problem of ultrasound waveform tomography is formulated in a ring-array transducer on S. The region of interest (ROI) is denoted by D. We start with the two-dimensional acoustical wave equation in heterogeneous media with the speed of sound $c(\mathbf{x})$ and the attenuation coefficient $\alpha(\mathbf{x})$,

$$-\frac{\partial^2 P(\mathbf{x},t)}{\partial t^2}+c^2(\mathbf{x})\nabla^2 P(\mathbf{x},t)+\alpha(\mathbf{x})\nabla^2\frac{\partial P(\mathbf{x},t)}{\partial t}=Q(\mathbf{x},t). \tag{1}$$

Where $P(\mathbf{x},t)$ is the pressure field at the location $\mathbf{x}$ and the time t, and $Q(t)$ denotes a pulse excitation from a point-like source located at $\mathbf{s}$. Note that the attenuation coefficient $\alpha(\mathbf{x})$ is temporally independent since only the pressure field has a relatively narrow band of frequencies. And in this section, the point-like sources and receivers are considered in order to validate the efficiency and robustness of the proposed algorithms. Hence, the main inverse problem of USCT is to recover the speed of sound $c(\mathbf{x})$ and attenuation coefficient $\alpha(\mathbf{x})$ images in $\mathbf{x}\in D$ given the pressure field $P(\mathbf{s},t)$ on $\mathbf{s}\in S$.

The aim of the CSI method is to linearize the original nonlinear waveform inversion model by adding two new variables which are composed by the functions of both the speed of sound and the attenuation coefficient, namely, a contrast function and a contrast source. Then one can solve a two-objective optimization problem with the use of the alternating minimization method. In terms of the robust CSI (RCSI) method proposed in [14], the total-variation (TV) regularization method is additionally chosen to preserve more edge information for the reconstructed image. Subsequently, the algorithm of the robust contrast source inversion with the automatic choice rule of regularization parameter (RCSI-ACR) applied to the single-frequency measured data was given in [5]. The automatic choice rule of regularization parameter is added to the alternating minimization method in order to update the regularization parameter with the iteration steps.

The idea of multi-frequency accelerating strategy is that it tries to achieve the rapid convergence result of the contrast function using the low-frequency data on a coarse grid, and then restart the RCSI-ACR method through utilizing the last iteration result and the high-frequency data on a fine grid, leading to the improvement of the resolution. This method is called frequency hopping which has been presented in [12]. We consider that the value of points per wavelength is fixed for all frequency components, for instance, less than twenty [2]. As the frequency increases while we do frequency hopping, the computational burden of RCSI-ACR enlarges gradually because of the increasing number of grids for each frequency component. Moreover, compared with RCSI-ACR using single-frequency data, this strategy significantly prevents the reconstruction from being trapped into a local minima [12].

The time-domain wavefield measurements are simulated by the K-wave toolbox [11]. Each source emanates a Gaussian pulse wave . The frequency-domain data are computed with the Fourier transform of the time-domain measurements. Additionally, the dataset are contaminated by the 5% standard Gaussian noise.

One starts with the first example by applying the single-frequency measured data. A fixed regularization parameter is fixed at 10^{-4} for RCSI and the automatic choice rule is starting at 10^{-4} for RCSI-ACR. For these two methods, one-maximal-step inner iteration is chosen. Figures 1(a)-1(c) show the imaging quality under different choice rules when the CSI methods terminate at sufficiently 400 outer iteration steps. Figures 1(b) and 1(c) indicate that RCSI-ACR reconstructs a sharper image than RCSI. Moreover, the artifact, which is attributed to the noisy boundary data we generated in the synthetic wavefield data, degraded the image reconstructed by RCSI-ACR in Fig. 1(e), in comparison with the true one in Fig. 1(a).

In terms of the multi-frequency accelerating strategy, one can concentrate on the performance test of the reconstruction with utilizing single frequency (SF) and multi-frequency (MF) datasets, respectively. In this numerical test, we extract ten samples of the equi-spaced frequencies from the dataset with respect to each receiver. These ten equi-spaced frequencies ($N=10$) sequentially range from 0.1 MHz to 0.3 MHz, covering the center frequency of 0.25 MHz. Meanwhile, a test on a single frequency dataset of 0.3 MHz is employed as a reference experiment for the conventional RCSI-ACR method. The comparison of the computation cost on the different datasets is illustrated in Fig. 2. We see that for the MF dataset with $K_{\max}=20$, the proposed method using multi-frequency accelerating strategy costs approximate 2.68 s per iteration, whereas for the case of the SF data with the frequency of 0.3 MHz the computational time per iteration rises to approximate 4.04 s. Moreover, after calculating several iteration steps, calculating on the MF dataset with larger $K_{\max}$ may have shorter computational time.

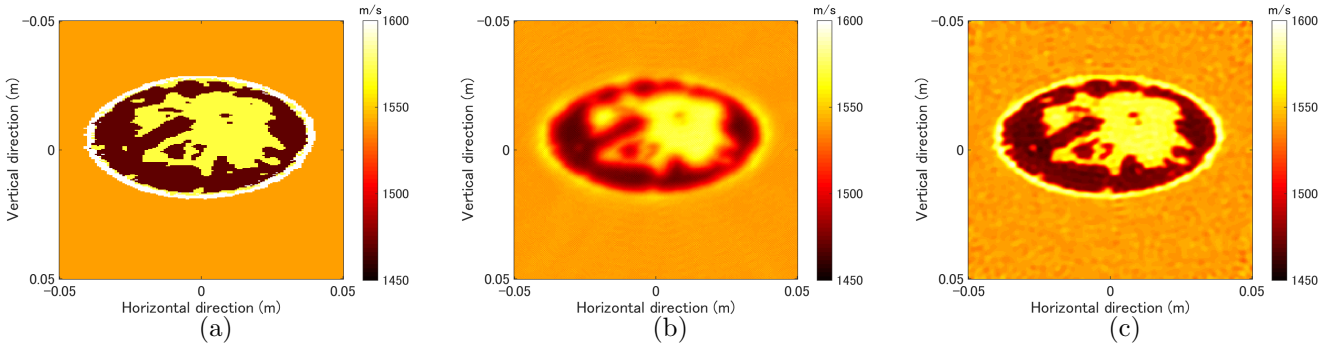

Figure 1: Speed of sound image of the medical phantom using (a) true model, (b) RCSI with 400 outer iteration steps, (c) RCSI-ACR with 400 outer iteration steps.

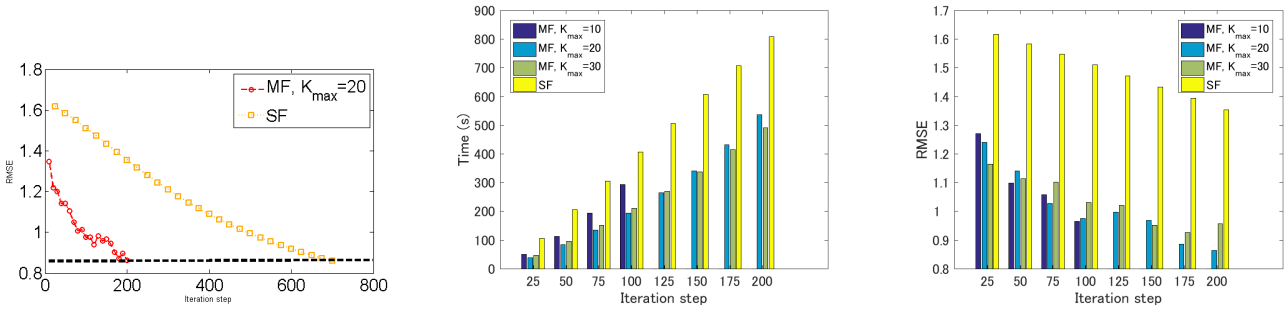

Figure 2: Computational time for the numerical solution of each iteration step using RCSI-ACR with multi-frequency accelerating strategy. The MF dataset with $K_{\max} = 10, 20, 30$ as well as the SF dataset with the frequency of 0.3 MHz are applied to the algorithm. (a) SF and MF reconstructions with the same stop criterion of RMSE. (b) Computational Time v.s. Iteration step. (c) RMSE v.s. Iteration step.

3 Ultrasound waveform tomography with finite sources/receivers – practical configuration

The wavefield dataset acquired from the ring transducer are able to apply to RCSI-ACR with the consideration of the configuration of finite sources/receivers. Each element of ultrasound transducer has its unique characteristics, such as direction and aperture. Minimum variance beamforming is a way to synthesize the finite source using the superposition of a number of the point-like sources. Meanwhile, the governing equation (1) should adapt to the configuration of finite sources/receivers by taking their acoustic properties into consideration.

The urethane phantom images are calculated by applying the experimental measurements acquired from the prototype of the ring transducer. Figure 3 shows that the structure of this defective hemisphere is successfully reconstructed by the attenuation image rather than the speed of sound image. This is because the calibration of the source/receiver locations is required to correct the phase information in the measurement. Moreover, the gap between the governing equation and the real phenomenon probably depends on the boundary condition related to the reflectivity of the ring transducer and the bad channels because of the intrinsic defects in the structure of transducer.

References

[1] A. Abubakar, W. Hu, P. Van Den Berg, and T. Habashy. A finite-difference contrast source inversion method. *Inverse Problems*, 24(6):065004, 2008.

[2] E. J. Alles and K. W. A. van Dongen. Perfectly matched layers for frequency-domain integral equation acoustic scattering problems. *IEEE Trans. Ultrason. Ferroelectr. Freq. Control*, 58(5):1077–1086, 2011.

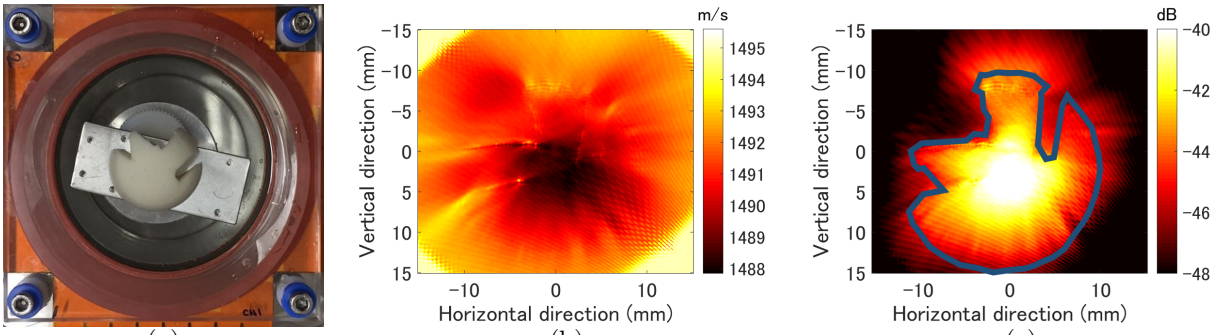

(a) (b) (c)

Figure 3: Ultrasound waveform tomography for the urethane phantom measurements: (a) the prototype of ring transducer with the urethane phantom, (b) the speed of sound image, (c) the attenuation coefficient image; solid line describes the base shape of the urethane phantom.

[3] N. Duric, G. Sandhu, O. Roy, C. Li, P. J. Littrup, M. Sak, and R. F. Brem. Toward high resolution whole breast imaging using ultrasound tomography: A comparison with mri. RSNA 2016 Annual Meeting, 2016.

[4] C. Li, G. S. Sandhu, O. Roy, N. Duric, V. Allada, and S. Schmidt. Toward a practical ultrasound waveform tomography algorithm for improving breast imaging. volume 9040 of *Proc. SPIE*, page 90401P, 2014.

[5] H. Lin, T. Azuma, X. Qu, and S. Takagi. Robust contrast source inversion method with automatic choice rule of regularization parameters for ultrasound waveform tomography. *Jpn. J. Appl. Phys.*, 55(7S1):07KB08, 2016.

[6] N. Ozmen-Eryilmaz. *Ultrasound Imaging Methods for Breast Cancer Detection.* PhD thesis, Laboratory of Acoustical Wavefield Imaging, Delft University of Technology, Delft, 2014.

[7] X. Qu, T. Azuma, H. Imoto, R. Raufy, H. Lin, H. Nakamura, S. Tamano, S. Takagi, S. I. Umemura, I. Sakuma, and Y. Matsumoto. Novel automatic first-arrival picking method for ultrasound sound-speed tomography. *Jpn. J. Appl. Phys.*, 54(7S1):07HF10, 2015.

[8] X. Qu, T. Azuma, H. Nakamura, H. Imoto, S. Tamano, S. Takagi, S.-I. Umemura, I. Sakuma, and Y. Matsumoto. Bent ray ultrasound tomography reconstruction using virtual receivers for reducing time cost. volume 9419 of *Proc. SPIE*, page 94190F, 2015.

[9] O. Roy, I. Jovanović, A. Hormati, R. Parhizkar, and M. Vetterli. Sound speed estimation using wave-based ultrasound tomography: theory and GPU implementation. volume 7629 of *Proc. SPIE*, page 76290J, 2010.

[10] G. Y. Sandhu, C. Li, O. Roy, S. Schmidt, and N. Duric. Frequency domain ultrasound waveform tomography: breast imaging using a ring transducer. *Phys. Med. Biol.*, 60(14):5381–5398, 2015.

[11] B. E. Treeby and B. T. Cox. k-Wave: MATLAB toolbox for the simulation and reconstruction of photoacoustic wave fields. *J. Biomed. Opt.*, 15(2):021314, 2010.

[12] P. M. van den Berg and A. Abubakar. Contrast source inversion method: State of art. *Progress in Electromagnetic Research*, 34:189–218, 2001.

[13] P. M. van den Berg and R. E. Kleinman. A contrast source inversion method. *Inverse Probl.*, 13(6):1607–1620, 1997.

[14] P. M. van den Berg, A. L. van Broekhoven, and A. Abubakar. Extended contrast source inversion. *Inverse Probl.*, 15(5):1325–1344, 1999.

[15] K. Wang, T. Matthews, F. Anis, C. Li, N. Duric, and M. Anastasio. Waveform inversion with source encoding for breast sound speed reconstruction in ultrasound computed tomography. *IEEE Trans. Ultrason. Ferroelectr. Freq. Control*, 62(3):475–493, 2015.

[16] L. Ying. Sparsifying preconditioner for the lippmann–schwinger equation. *Multiscale Model Simul.*, 13(2):644–660, 2015.